Photophysics and Nonlinear Absorption of Peripheral-Substituted Zinc Phthalocyanines

Yunjing Li,[†] Timothy M. Pritchett,[‡] Jiandong Huang,[§] Meirong Ke,[§] Pin Shao,[†] and Wenfang Sun*,[†]

Department of Chemistry and Molecular Biology, North Dakota State University, Fargo, North Dakota 58105-5516, U.S. Army Research Laboratory, AMSRD-ARL-SE-EM, 2800 Powder Mill Road, Adelphi, Maryland 20783-1197, and College of Chemistry and Chemical Engineering, Fuzhou University, Fuzhou 350002, China

Received: November 14, 2007; Revised Manuscript Received: May 9, 2008

The photophysical properties, such as the UV−vis absorption spectra, triplet transient difference absorption spectra, triplet excited-state extinction coefficients, quantum yields of the triplet excited state, and lifetimes of the triplet excited state, of 10 novel zinc phthalocyanine derivatives with mono- or tetraperipheral substituents have been systematically investigated in DMSO solution. All these complexes exhibit a wide optical window in the visible spectral range and display long triplet excited-state lifetimes (140−240 μs). It has been found that the complexes with tetrasubstituents at the α-positions exhibit a bathochromic shift in their UV−vis absorption spectra, fluorescence spectra, and triplet transient difference absorption spectra and have larger triplet excited-state absorption coefficients. The nonlinear absorption of these complexes has been investigated using the *Z*-scan technique. It is revealed that all complexes exhibit a strong reverse saturable absorption at 532 nm for nanosecond and picosecond laser pulses. The excited-state absorption cross sections were determined through a theoretical fitting of the experimental data using a five-band model. The complexes with tetrasubstituents at the α-positions exhibit larger ratios of triplet excited-state absorption to ground-state absorption cross sections (σ_T/σ_g) than the other complexes. In addition, the wavelength-dependent nonlinear absorption of these complexes was studied in the range of 470−550 nm with picosecond laser pulses. All complexes exhibit reverse saturable absorption in a broad visible spectral range for picosecond laser pulses. Finally, the nonlinear transmission behavior of these complexes for nanosecond laser pulses was demonstrated at 532 nm. All complexes, and especially the four α-tetrasubstituted complexes, exhibit stronger reverse saturable absorption than unsubstituted zinc phthalocyanines due to the larger ratio of their excited-state absorption cross sections to their respective ground-state absorption cross sections.

Introduction

Phthalocyanines (Pcs) and metallophthalocyanine (MPcs) have attracted great attention in the past few decades because of their versatile applications in materials science and biomedicine. For example, Pcs and MPcs have been utilized as industrial dyes,[1] photosensitizers for photodynamic therapy,[2] organic field-effect transistors,[3] photocatalysts,[4] and optical data storage materials.[5] In the past 20 years, there has been a growing interest in the nonlinear optical properties of these complexes due to the presence of an extensively delocalized π-electron system and the planar configuration in these complexes. In addition, the structures of Pcs and MPcs can be easily modified without changing their stability and processibility features. By introducing different substituents at the peripheral position of the macrocyclic ring, varying the central metal, alternating the axial ligand, or changing the symmetry of the macrocycle, the photophysical and photochemical properties of these complexes can be influenced drastically.[6–11] It has been found that peripheral substituents can influence the electron delocalization, reduce aggregation, and enhance intersystem crossing in the case of heavy-atom substitution.[12,13] Axial substitution not only alters the electronic structure and the intermolecular interactions of the complex but also introduces an additional dipole moment perpendicular to the macrocyclic plane.[14] These steric and electronic feature changes could significantly impact the nonlinear optical properties of Pcs.[9]

It is well-known that various nonlinear optical processes can give rise to nonlinear transmission, in which the transmission remains constant when the incident light fluence is low but decreases at increasing incident light levels. Nonlinear transmission shows potential applications in laser pulse shaping (such as passive mode lock, laser pulse smoothing, stabilization, and compression), rejection of constant background in spectroscopy, and optical switching. Both nonlinear absorption (particularly reverse saturable absorption and multiphoton absorption) and nonlinear refraction can contribute to a change in transmission. For an ideal reverse saturable absorber, the material needs to have an appreciable ground-state absorption cross section to populate the excited state, a large ratio of excited-state to ground-state absorption cross sections, and a long excited-state lifetime. In the case of triplet excited-state absorption dominating reverse saturable absorption, the material needs to possess a high quantum yield of formation of the triplet excited state, i.e., a rapid intersystem crossing (isc). For practical use, it is desirable that the reverse saturable absorber exhibits a broadband spectral and temporal response and is transparent in the visible and the near-IR region.[15] The nonlinear absorption of a variety of organic and inorganic materials has been investigated since the 1960s. Among those investigated

* Corresponding author. E-mail: Wenfang.Sun@ndsu.edu.
[†] North Dakota State University.
[‡] U.S. Army Research Laboratory.
[§] Fuzhou University.

10.1021/jp7108835 CCC: $40.75
Published on Web 07/11/2008

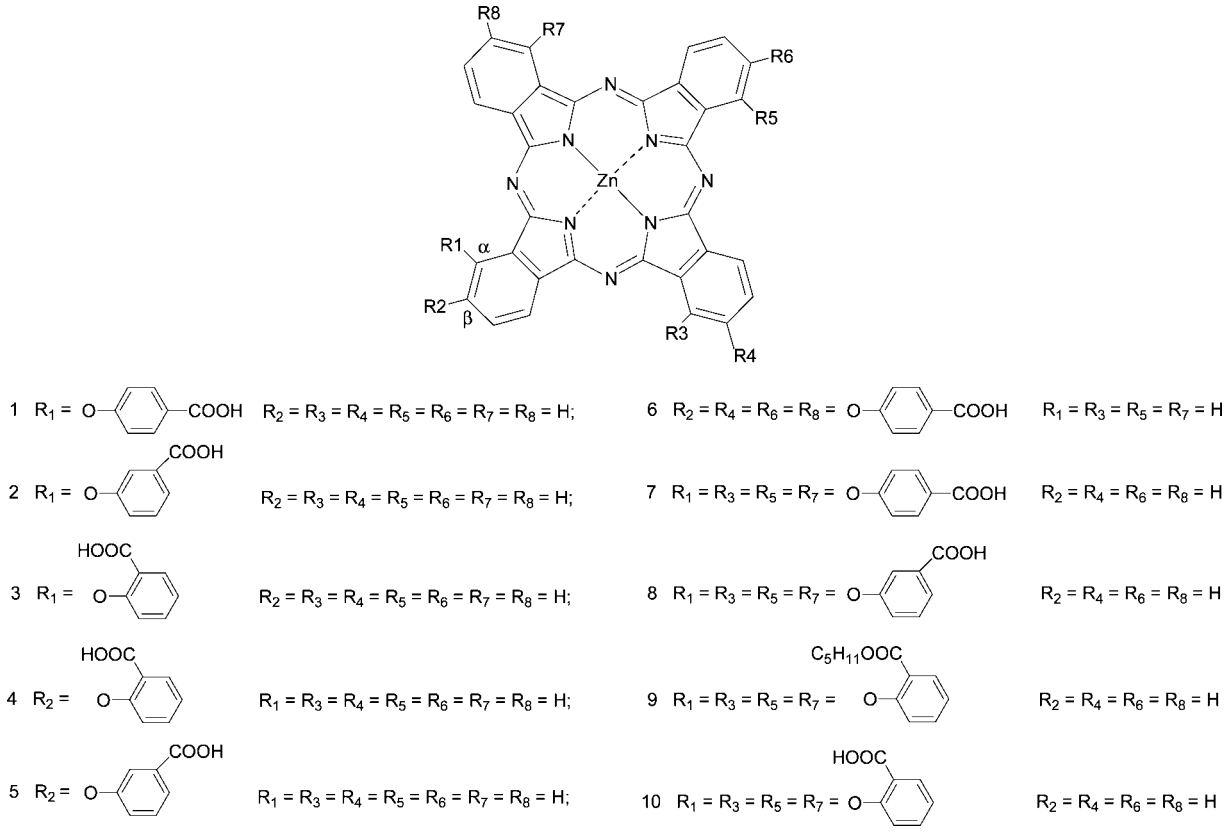

Figure 1. Structures of ZnPc derivatives.

materials, phthalocyanines and derivatives have been reported to exhibit reverse saturable absorption for both nanosecond and picosecond laser pulses[13,14,16–18] and a fairly wide optical window in the visible to the near-IR region between the Q- and B-bands. The most attractive feature of Pcs is their large ratio of the excited-state absorption cross section (σ_{ex}) to the ground-state absorption cross section (σ_g). In addition, Pcs with heavy central metal ions, such as Pb and In, have been found to possess a larger yield of triplet excited-state formation due to heavy-atom enhanced isc.[18] All these features make Pcs a class of promising nonlinear transmission materials.

Although there have been extensive reports on the nonlinear optical properties of Pcs using nanosecond or picosecond lasers,[6,14,19] the Pcs that exhibit strong nonlinear absorption usually possess heavier metals. The optical nonlinearities of ZnPc derivatives have not been extensively explored. In particular, the effect of peripheral substituents is not well understood. Furthermore, the reported work on ZnPcs was conducted either at 532 or 1064 nm. The wavelength dispersion of the nonlinear absorption of ZnPcs has not been studied yet. Therefore, in this work the nonlinear absorption of 10 ZnPc derivatives (structures shown in Figure 1) with different numbers of peripheral substituents and with substituents occupying the different positions of the macrocyclic ring were investigated using the open-aperture *Z*-scan technique at both nanosecond and picosecond time regimes. The effects of the number and position of the peripheral substituents on the triplet transient difference absorption spectra, extinction coefficients, triplet quantum yields, and lifetimes of the triplet excited state of these ZnPc derivatives were also systematically studied. It is our intention to build up the correlations between these photophysical parameters and the nonlinear absorption of these ZnPc derivatives for the future rational design of phthalocyanines with broad and strong nonlinear absorption.

Experimental Section

Materials. All the ZnPc derivatives used in this study were provided by Professor Jiandong Huang's group at Fuzhou University, China. All samples were characterized by UV−vis, NMR, and mass spectrometry. The details of the synthesis and characterization will be published elsewhere.[20] The reference material ZnPc and ZnTPP were purchased from Aldrich Inc. and Alfa Aesar Company, respectively, and used as is. The solvent DMSO was obtained from Alfa Aesar Company and used as received without further purification.

Photophysical Measurements. All of the photophysical measurements were carried out in DMSO solutions. The UV−vis spectra were recorded on an Agilent 8453 UV−vis spectrophotometer in a 1 cm quartz cuvette. The fluorescence spectra were measured on a SPEX Fluorolog-3 fluorometer. The singlet excited-state lifetimes were measured using the time-correlated single photon counting technique. Each sample was excited at 375 nm with an approximate 70 ps pulsewidth, and the emission was monitored at the wavelength of the emission band maximum. The instrument response time (IRT) was measured to be 130 ps [full width at half-maximum (fwhm)] using a colloidal silica suspension (called Snowtex) diluted with water and setting the emission monochromator at the excitation wavelength, i.e., 375 nm. The concentrations of the solutions were adjusted to obtain an absorbance of ~0.1 at 375 nm. The fluorescence quantum yields of the samples were determined by the comparative method;[21] ZnPc ($\Phi_f = 0.23$ in DMSO)[22] was used as the reference. The absorbances of the samples and the reference were all adjusted to ~0.07 at the excitation wavelength 610 nm.

The triplet transient difference absorption spectra, the triplet excited-state lifetimes, the triplet−triplet molar extinction coefficients, and the triplet quantum yields were measured on an Edinburgh LP920 laser flash photolysis spectrometer. The third-harmonic output (355 nm) of a Q-switched Nd:YAG laser (Quantel Brilliant, pulsewidth (fwhm) = 4.1 ns, repetition rate = 1 Hz) was used as the excitation source. The sample solutions were purged with argon for at least 30 min before each measurement.

The triplet−triplet absorption coefficients (ε_T) of the samples were obtained using the singlet depletion method,[23] and the following equation was used to calculate the ε_T.

$$\varepsilon_T = \frac{\varepsilon_S \Delta OD_T}{\Delta OD_S} \quad (1)$$

where ΔOD_S and ΔOD_T are the optical density change of the triplet transient difference absorption spectrum at the minimum of the bleaching band and the maximum of the positive band, respectively, and ε_S is the ground-state molar extinction coefficient at the UV−vis absorption band maximum. Both ΔOD_S and ΔOD_T were obtained from the triplet transient difference absorption spectra.

The triplet quantum yield Φ_T was obtained by comparing the ΔOD of the optically matched sample solution at 355 nm in a 1 cm cuvette to that of the reference material, ZnPc (Φ_T = 0.65 ± 0.02, ε_{480} = 30 000 ± 1000 M^{-1} cm^{-1}),[22] at 480 nm using the equation[24]

$$\Phi_T^S = \Phi_T^{ZnPC} \frac{\Delta OD_T^S}{\Delta OD_T^{ZnPC}} \times \frac{\varepsilon_T^{ZnPC}}{\varepsilon_T^S} \quad (2)$$

where the superscript s represents the samples, ΔOD is optical density of the triplet transient difference absorption spectrum at 480 nm, and ε_T is the triplet excited-state extinction coefficient.

The singlet oxygen quantum yield (Φ_Δ) was determined by measuring the emission of $^1O_2$ in air-saturated DMSO solution using an Edinburgh TL900 transient luminescence spectrometer that is equipped with an ultrafast and ultrasensitive EI-P germanium detector. The third-harmonic output (355 nm) of the Quantel Nd:YAG laser was used as the excitation source. A silicon cutoff filter (the transmission at $\lambda > 1180$ nm is ~52%, and the transmission at 1064 nm is approximately 35%) was used to reduce the scattered light from the YAG laser. The quantum yield of the singlet oxygen generation was calculated by comparing the singlet oxygen emission intensity of the sample solution to that of a reference material (ZnTPP, Φ_Δ = 0.94 in toluene)[25] according to eq 3[26]

$$\Phi_\Delta^S = \Phi_\Delta^{REF} \times \left(\frac{n_S}{n_{REF}}\right)^2 \frac{G_\Delta^S}{G_\Delta^{REF}} \times \frac{A_{REF}}{A_S} \quad (3)$$

where G_Δ is the integrated emission intensity, A is the absorbance of the sample at 355 nm, and n is the refractive index of the solvent. REF and S refer to the reference material ZnTPP and to ZnPc derivatives, respectively.

Z-Scan Measurements and Fittings. The open-aperture *Z*-scan experimental setup is shown in Figure 2. For nanosecond *Z*-scan experiments, the second-harmonic output (532 nm) of a Q-switched Quantel Brilliant Nd:YAG laser was used as the light source. The laser pulsewidth was 4.1 ns (fwhm), and the repetition rate was adjusted to 10 Hz. The spatial profile of the laser beam was a nearly Gaussian distribution. The beam was focused by a plano−convex lens with a focal length of 30 cm. The radius of the beam waist at HW/e^2 was measured to be 32 μm using a knife edge; this corresponds to a Rayleigh length of 6.0 mm. Therefore, the sample in the 1 mm thick cuvette can be treated as a thin sample. For the picosecond *Z*-scan experiments, the laser source was an optical parametric oscillator (OPO) (EKSPLA PG 401) pumped by the third harmonic of a Nd:YAG laser (EKSPLA PL 2143A). The laser pulsewidth was 27 ps (fwhm), and the repetition rate was 10 Hz. The focal length of the plano−convex lens was 15 cm, resulting in a beam waist (HW/e^2) of ω_0 = 40 μm at 532 nm measured by a knife edge. In both nanosecond and picosecond *Z*-scan measurements, the energy of the transmitted beam after the sample was measured by detector D2, while the incident laser beam energy was monitored by detector D1. The sample was mounted on a translation stage (Newport M-UTM100) and moved through the vicinity of the focal plane. A computer was used to control the translation stage movement and the data acquisition.

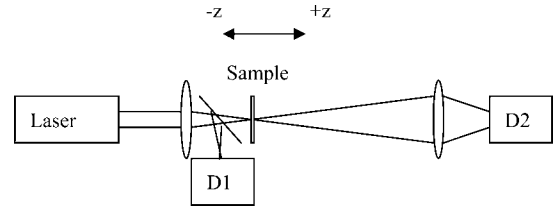

Figure 2. Configuration of the open-aperture *Z*-scan experiment.

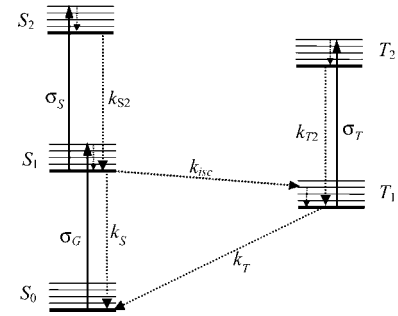

Figure 3. Five-band model.

To fit the open-aperture *Z*-scan experimental data, a five-band model depicted in Figure 3 was used. Each molecule is assumed to lie in the vibration−rotation manifold of one of five electronic states: the ground state, S_0, a singlet; one of two excited singlet states, S_1 or S_2; or one of two excited triplet states, T_1 or T_2. The following rate equations describe the time evolution of the number densities n_G, n_S, n_T, and n_{S2} of molecules in S_0, S_1, T_1, and S_2 bands, respectively.

$$\frac{\partial n_G}{\partial t} = -\frac{\sigma_G}{h\nu} n_G I + k_S n_S + k_T n_T \quad (4a)$$

$$\frac{\partial n_S}{\partial t} = \frac{\sigma_G}{h\nu} n_G I - (k_S + k_{isc}) n_S - \frac{\sigma_S}{h\nu} n_S I + k_{S2} n_{S2} \quad (4b)$$

$$\frac{\partial n_T}{\partial t} = k_{isc} n_S - k_T n_T - \frac{\sigma_T}{h\nu} n_T I + k_{T2} n_{T2} \quad (4c)$$

$$\frac{\partial n_{S2}}{\partial t} = \frac{\sigma_S}{h\nu} n_S I - k_{S2} n_{S2} \quad (4d)$$

(n_{T2} is obtained from the constraint $n_0 = n_G + n_S + n_T + n_{S2} + n_{T2}$, where n_0 is the total number of molecules per unit volume.) Here, σ_G, σ_S, and σ_T denote absorption cross sections and k_S, k_{S2}, k_T, k_{T2}, k_{isc} are rate constants for nonradiative decays, ν is the frequency of the laser radiation, h is the Planck constant,

and I is the irradiance. The following extinction law describes the diminution of the irradiance with distance z as the pulse propagates through the sample:

$$\frac{\partial I}{\partial z} = -(\sigma_G n_G + \sigma_S n_S + \sigma_T n_T) I \quad (5)$$

In order to account for the spatial variation of the molecular band populations and the pulse irradiance within the sample, the sample region was divided into a series of longitudinal slices of thickness Δz. Consistent with the assumed cylindrical symmetry of the laser beam, each slice was further divided into a series of concentric annular regions, with a disk-shaped region at the center. The band populations (n_i) were taken to be the same within any given region; in effect, the sample was replaced with a two-dimensional (z, r) grid. Beginning at the input face of the sample, the following procedures were taken on each longitudinal slice in turn. At each radial grid point on the slice, eqs 4a–4d were first solved numerically, and $I(z, r; t)$, the irradiance at that point, was treated parametrically (thus neglecting the effects of irradiance depletion as the pulse propagates through the slice in question). The newly obtained ($n_i(z, r; t)$) were then inserted in eq 5, and the pulse depletion by the slice was computed. The resulting irradiance $I(z + \Delta z, r; t)$ serves as the input at the corresponding radial grid point on the next slice. This procedure is justified on physical grounds: by taking a sufficiently large number of longitudinal slices, one can make each slice so thin that the irradiance depletion from that slice is negligible, as is the error incurred by effectively decoupling eqs 4a–4d and 5 and first solving eqs 4a–4d while disregarding the effects of irradiance depletion from the slice.

In fitting the Z-scan data reported in the Results and Discussion section, the decays from the higher excited bands, both singlet and triplet, to the corresponding first excited bands were assumed to be ultrafast, as were decays to the lowest-lying vib−ro level in any band. Experimentally measured values for the S_1 lifetime k_S^{-1}, the T_1 lifetime k_T^{-1}, and the triplet quantum yield Φ_T were employed in the model in order to obtain a single pair of excited-state absorption cross section values (σ_S, σ_T) that simultaneously fit both the nanosecond and picosecond Z-scans.

Nonlinear Transmission Measurement. The nanosecond nonlinear transmission experimental setup was previously described in detail.[27] The Quantel Brilliant Nd:YAG laser was used as the light source and operated at its second-harmonic output (532 nm) with a 10 Hz repetition rate. The incident energy was tuned by the combination of a polarizing cube beam splitter, a half-wave plate, and a sheet polarizer. The thickness of the sample cell was 2 mm, and the radius of the beam (HW/e^2) was measured to be ~72 μm by a knife edge. Two Molectron J4-09 pyroelectric joulemeters were used as the probes for monitoring the incident and output energies.

Results and Discussion

UV Absorption Spectra. The UV−vis absorption spectra of ZnPc derivatives in DMSO are presented in Figure 4. The molar extinction coefficients at the band maxima and the oscillator strengths for the B- and Q-bands calculated from the Gaussian fit are listed in Table 1. All complexes exhibit B-band(s) and Q-bands in the visible and near-IR region, respectively, with the Q(0,0) bands red-shifted relative to those of the unsubstituted ZnPc.[28] The tetrasubstituted complexes with substituents occupying the α-position (**7**−**10**) exhibit an approximately 15 nm red-shift of their Q(0,0) bands and 20 nm red-shift of their B-bands compared to the five monosubstituted

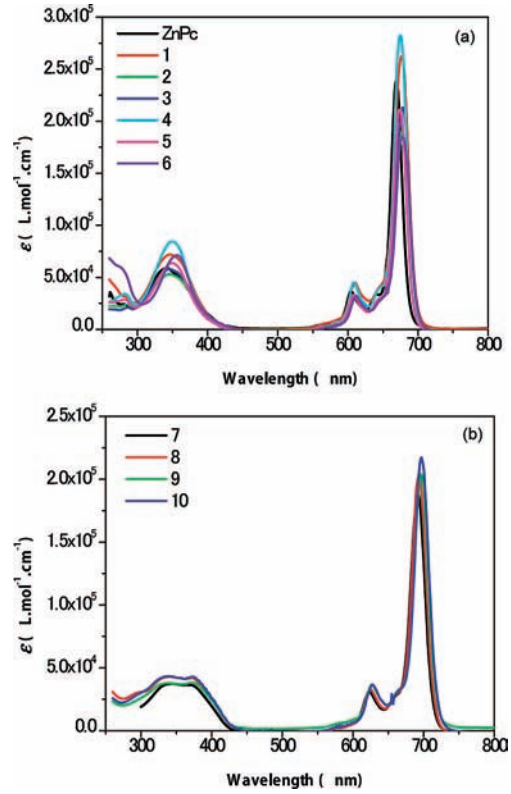

Figure 4. UV−vis absorption spectra of ZnPc derivatives in DMSO. (a) ZnPc and complexes **1**−**6**; (b) complexes **7**−**10**. The y-axis is the molar extinction coefficient (ε).

complexes **1**−**5** and the tetrasubstituted one with substituents occupying the β-position (**6**); meanwhile the B-bands of **7**−**10** show the vibronic structure. A close examination of the five monosubstituted complexes **1**−**5** reveals that complexes **4** and **5**, which have the substituent at β-position, show a 3 nm red-shift in their B-bands, but a 3 nm hypsochromic shift in their Q(0,0) bands compared to complexes **1**−**3** with α-substitution. Interestingly, the UV−vis spectrum of tetrasubstituted complex **6** with substituents located at the β-positions is quite distinct from complexes **7**−**10** that have the four substituents at the α-positions. Its spectrum resembles those of the monosubstituted complexes **1**−**5**, with a 7−11 nm red-shift of its B-band. Therefore, both the number and the position of the substituents on the peripheral ring of phthalocyanines affect the absorption spectra of ZnPc derivatives. The red-shift of the absorption bands in **7**−**10** could probably arise from the nonplanarity caused by the steric hindrance of the substituents at the α-positions. However, no X-ray diffraction data is available to confirm this speculation at this time. In contrast, different substituent type (*o*-, *m*-, *p*-carboxylphenoxy or pentyl carboxylphenoxy) exhibits a negligible effect on the UV−vis spectra. In addition, the Q(0,0) bands of all complexes are quite narrow and intense, and the Beer−Lambert law is followed for both the Q-band and the B-band in the concentration range used in our studies (10^{-6} to 10^{-4} mol/L), indicating that no aggregation occurs in this concentration range.[29]

It is valuable to point out that all complexes possess a fairly broad "transparency window" between 425 and 575 nm, where the typical ground-state absorption cross section (σ_g) is of the order of 10^{-19} to 10^{-18} cm^2. According to the studies on other phthalocyanines, reverse saturable absorption (RSA) is expected to occur in this spectral range, as will be demonstrated by the open-aperture Z-scans and the nonlinear transmission measurements presented later in this paper.

TABLE 1: Photophysical Data of ZnPc Derivatives in DMSO

complex	λ_{abs}/nm (ε/10^4 L·mol^{-1}·cm^{-1}, f[a])	λ_f/nm (τ_s/ns, Φ_f)	λ_{T1-Tn}/nm (ε_{T1-Tn}/10^4 L·mol^{-1}·cm^{-1})	τ_T/μs	τ_{isc}/ns[b]	Φ_T	Φ_Δ[c]
ZnPc	343 (5.88, 1.59), 672 (24.0, 0.44)[d]	684 (3.66, 0.23[e])	480 (3.00 ± 0.10)[e]	123 ± 9	5.63	0.65 ± 0.02[e]	0.67[f]
1	346 (7.21, 1.99), 677 (26.3, 0.51)	684 (3.01, 0.14)	500 (5.02 ± 0.05)	200 ± 9	7.92	0.38 ± 0.01	0.18
2	345 (5.31, 1.58), 677 (19.0, 0.37)	684 (3.11, 0.12)	480 (3.70 ± 0.28)	168 ± 27	6.35	0.49 ± 0.04	0.17
3	346 (5.80, 1.99), 678 (21.3, 0.41)	684 (3.10, 0.11)	480 (4.31 ± 0.31)	170 ± 18	7.75	0.40 ± 0.03	0.19
4	349 (8.45, 2.40), 675 (28.2, 0.61)	680 (3.17, 0.15)	480 (4.82 ± 0.49)	181 ± 27	7.93	0.40 ± 0.04	0.14
5	349 (6.37, 1.59), 674 (21.1, 0.46)	680 (3.27, 0.16)	480 (3.82 ± 0.15)	161 ± 40	7.98	0.41 ± 0.02	0.15
6	356 (7.13, 1.57), 678 (18.5, 0.44)	686 (3.00, 0.10)	500 (2.96 ± 0.11)	238 ± 40	6.12	0.49 ± 0.02	0.17
7	340 (3.75, 1.20), 371 (3.63, 0.29), 692 (20.9, 0.44)	700 (2.70, 0.06)	560 (11.1 ± 0.48)	215 ± 21	7.11	0.38 ± 0.02	0.31
8	341 (4.29, 1.91), 371 (4.20, 0.17), 693 (20.2, 0.47)	700 (2.70, 0.06)	560 (12.1 ± 0.35)	174 ± 21	6.59	0.41 ± 0.01	0.30
9	337 (3.79, 1.17), 372 (3.83, 0.33), 696 (20.4, 0.44)	702 (2.59, 0.06)	560 (20.4 ± 0.82)	142 ± 8	10.4	0.25 ± 0.01	0.36
10	340 (4.33, 1.62), 374 (4.29, 0.35), 697 (21.7, 0.50)	704 (2.83, 0.06)	560 (18.4 ± 1.17)	140 ± 5	11.8	0.24 ± 0.02	0.39

[a] Oscillator strength, $f = (4.3 \times 10^{-9}) \int \nu \, d\nu$. [b] $\tau_{isc} = \tau_s/\Phi_T$. [c] The uncertainty is ±0.01. [d] From ref 28. [e] From ref 22. [f] From ref 31.

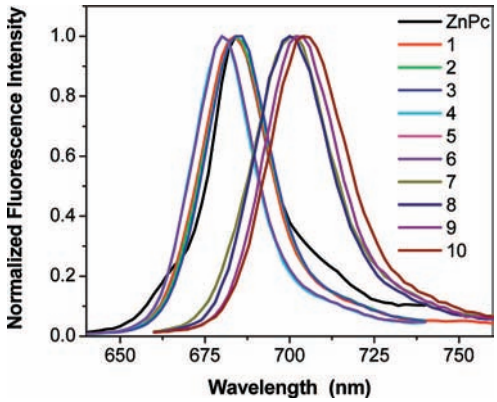

Figure 5. Normalized fluorescence spectra of ZnPc and its derivatives in DMSO. The excitation wavelength is the Q(0,0) band maximum for each sample.

Singlet Excited-State Characteristics. Figure 5 displays the fluorescence spectra of the ZnPc derivatives in DMSO solutions when excited at the corresponding Q(0,0) band maximum for each sample. Exactly the same emission spectra were obtained for a 375 nm excitation, which is within the B-band region. Similar to the trend observed from the UV−vis absorption spectra that are discussed in the previous section, the emission spectra of complexes **1**−**10** are divided into two groups: the emission band maxima of **1**−**6** appear at ∼680 nm, whereas the band maxima red-shift to ∼700 nm for **7**−**10**. Considering the mirror image of the emission bands to the Q(0,0) bands in the UV−vis absorption spectra and the small Stokes shift (5−8 nm), the emission should originate from the lowest vibronic state of the first singlet excited state. In line with this assignment, the singlet excited-state lifetimes measured using the time-correlated single photon counting (TCSPC) technique are approximately 3 ns, with **1**−**6** exhibiting a slightly longer lifetime than **7**−**10**. With the use of the unsubstituted ZnPc as the reference, the fluorescence quantum yield was determined to be 0.10−0.14 for **1**−**6**, and 0.06 for **7**−**10**.

Triplet Excited-State Characteristics. As discussed in the previous section, the UV−vis absorption spectra of the ZnPc derivatives display a broad "transparency window" between their B-bands and Q-bands. Therefore, RSA is expected to be observed in this spectral range. To demonstrate this, the triplet transient difference (TA) absorption spectra that measure the absorption difference between the triplet excited state and the ground state of these complexes were investigated. Positive bands in the TA spectrum usually suggest a triplet excited-state absorption that is stronger than that of the ground state, and thus RSA can take place in those spectral regions. A bleaching band indicates the opposite case. Additionally, the decay of the transient absorption at a given wavelength contains information on the decay of the triplet excited state, from which the triplet excited-state lifetime can be deduced.

Figure 6 shows the triplet transient difference absorption spectra of the 10 ZnPc derivatives right after excitation. Similar to what is observed in the UV−vis and fluorescence spectra, the TA spectra of these complexes are divided into two groups. Complexes **1**−**6** display positive bands from 390 to 600 nm and bleaching bands from 610 to 800 nm, whereas the positive bands for complexes **7**−**10** appear at 410−610 nm and the bleaching bands at 620−800 nm. The location of the positive bands corresponds to the "transparency window" observed in the UV−vis spectra, whereas the bleaching band coincides with the spectral region of the Q-band. In line with the trend discovered in the UV−vis and fluorescence spectra, the maxima of the positive bands red-shift from 480 nm for **1**−**6** to 560 nm for **7**−**10**. Moreover, this trend is observed not only for the energy of the $T_1 - T_n$ absorption but also extends to the molar extinction coefficients (ε_{T1-Tn}) of the $T_1 - T_n$ absorption. As shown in Table 1, the ε_{T1-Tn} values obtained from the singlet depletion method[21] for **7**−**10** are 2−6 times as large as those for **1**−**6**. This suggests that α-tetrasubstitution not only decreases the transition energies of $S_0 \rightarrow S_1$ and $T_1 \rightarrow T_n$ but also increases the transition probability of $T_1 \rightarrow T_n$.

Figure 7 shows the representative time-resolved transient difference absorption spectra of two complexes. By analyzing the decay of the transient absorption, one determines the lifetime of the triplet excited state (τ_T). As listed in Table 1, the lifetimes of all complexes are quite long, on the order of hundreds of microseconds, which is significantly longer than that of the unsubstituted ZnPc. On the basis of eq 2, the quantum yields for formation of the triplet excited state are determined to be 0.38−0.49 for **1**−**8**, and ∼0.24 for **9** and **10**. Although these values are not as large as that for ZnPc, the larger triplet excited-state absorption coefficients/cross sections (see ε_{T1-Tn} in Table 1 and the σ_T values at 532 nm in Table 2) would be able to compensate for these reduced Φ_T values and result in better nonlinear transmission performance (see Figure 9 and the discussion in Nonlinear Transmission section). In addition, these values, along with the singlet excited-state lifetimes measured by the TCSPC technique (listed in Table 1) are used to calculate the isc times ($\tau_{isc} = \tau_s/\Phi_T$), which results in ∼6−8 ns for **1**−**8** and ∼10−12 ns for **9** and **10** (see Table 1). Since these isc

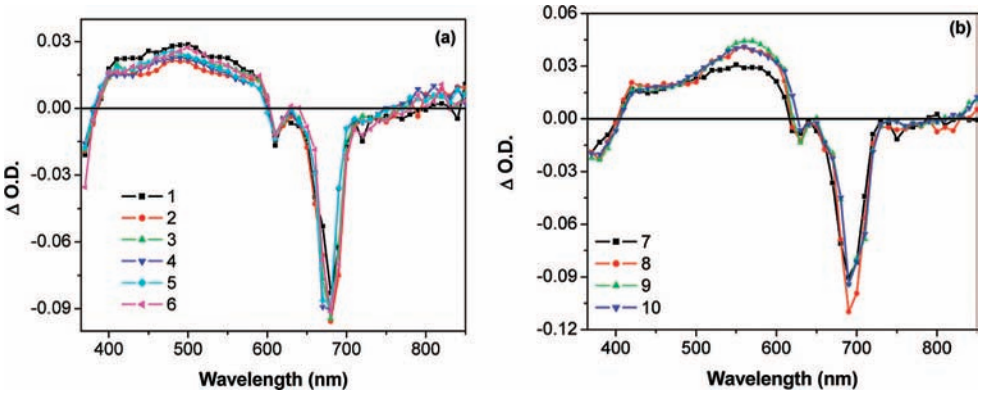

Figure 6. Triplet transient difference absorption spectra of the ZnPc derivatives immediately after the excitation. $\lambda_{ex} = 355$ nm; the excitation is provided by the 4.1 ns (fwhm) Nd:YAG laser. (a) Complexes **1**−**6**; (b) complexes **7**−**10**.

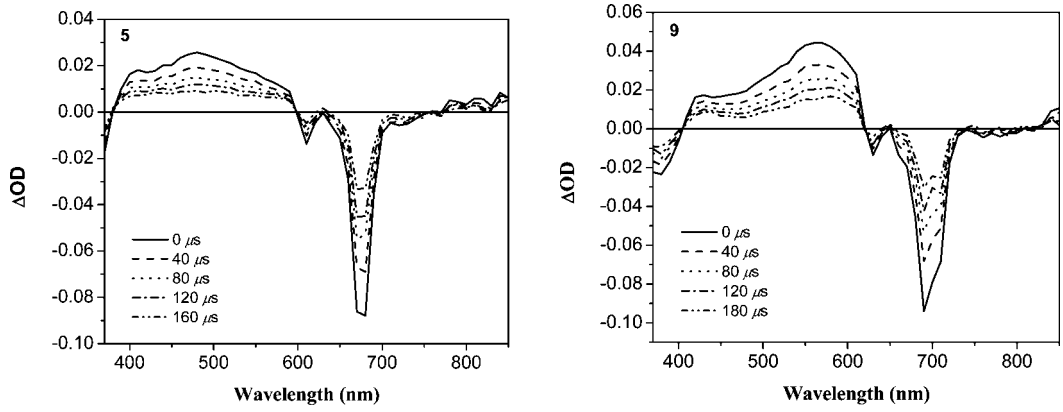

Figure 7. Time-resolved triplet transient difference absorption spectra of **5** and **9** in DMSO. $\lambda_{ex} = 355$ nm. The legend indicates the delay time after excitation.

TABLE 2: Excited-State Absorption Cross Sections of ZnPc Derivatives in DMSO Measured by Open-Aperture *Z*-Scans at 532 nm

complex	$\sigma_g/10^{-18}$ cm^2	$\sigma_s/10^{-17}$ cm^2	$\sigma_T/10^{-17}$ cm^2	σ_s/σ_g	σ_T/σ_g
1	3.1	4.0 ± 0.5	18.0 ± 2.0	13	58
2	2.4	4.0 ± 0.5	10.5 ± 2.0	17	44
3	2.5	4.5 ± 0.5	7.0 ± 1.5	18	28
4	3.7	4.5 ± 0.8	11.0 ± 2.0	12	30
5	3.1	4.5 ± 0.5	6.0 ± 1.5	15	19
6	4.0	4.0 ± 0.6	4.5 ± 1.0	10	11
7	1.6	3.0 ± 0.5	17.0 ± 2.0	19	106
8	2.3	1.8 ± 0.4	18.0 ± 2.5	8	78
9	1.3	1.8 ± 0.2	40.0 ± 4.0	14	308
10	1.8	3.0 ± 0.5	28.0 ± 3.0	17	156

times are of the same order as the pulsewidth of the nanosecond laser used for the nonlinear optical measurements, the nanosecond *Z*-scan and nonlinear transmission studies that will be discussed in the following two sections include contributions from both the singlet and the triplet excited states.

The quantum yields for singlet oxygen generation were measured to be 0.14−0.19 for **1**−**6** and 0.30−0.39 for **7**−**10**. It is quite obvious that the energy transfer efficiencies ($S_\Delta = \Phi_\Delta/\Phi_T$) from the triplet excited-state to the ground-state oxygen are much higher for **7**−**10** than for **1**−**6**. It is noted that the singlet oxygen quantum yields of **9** and **10** are higher than their triplet excited-state quantum yields. This is possibly due to the error in the triplet absorption coefficient measurement, in which the singlet depletion method usually gives an upper bound to the value of ε_T;[23,30] the higher ε_T value subsequently induces a lower Φ_T. The higher-than-expected value of ε_T could possibly be due to the ground-state extinction coefficients that are not negligible at the transient absorption spectrum band maximum ($\lambda = 560$ nm). On the other hand, the fact that Φ_Δ is larger than Φ_T could also possibly be due to energy transfer from a higher triplet excited-state to the ground-state oxygen, since the excitation wavelength used for the singlet oxygen measurement was 355 nm. Unfortunately, the limitations of our instrument made it impossible to excite the samples at the Q(0,0) band in order to exclude the possibility of energy transfer from a higher triplet excited state. Nevertheless, the fact that the value of S_Δ for these two complexes is very nearly unity suggests that energy transfer efficiency from the triplet excited-state to the ground-state oxygen is quite high.

***Z*-Scan Measurement.** The *Z*-scan technique can measure the nonlinear absorption and nonlinear refraction simultaneously, and the contribution from nonlinear absorption and nonlinear refraction can be separated through data analysis. In *Z*-scan experiments, the transmittance of the sample in the far field is monitored as a function of the sample position relative to the linear focal plane. In the absence of an aperture (referred as open-aperture *Z*-scans), the measurement determines the contribution purely from nonlinear absorption. Measurements using nanosecond and picosecond laser pulses would provide information on the triplet and singlet excited states, respectively. In general, when the laser pulsewidth is comparable to the isc time, as is true of nanosecond laser pulses in the case of most materials, *Z*-scans measure contributions from both the triplet and the singlet excited states, and when the laser pulsewidth is much shorter than the isc time, as is typically the case for picosecond pulses, the contributions from the singlet excited state dominate.

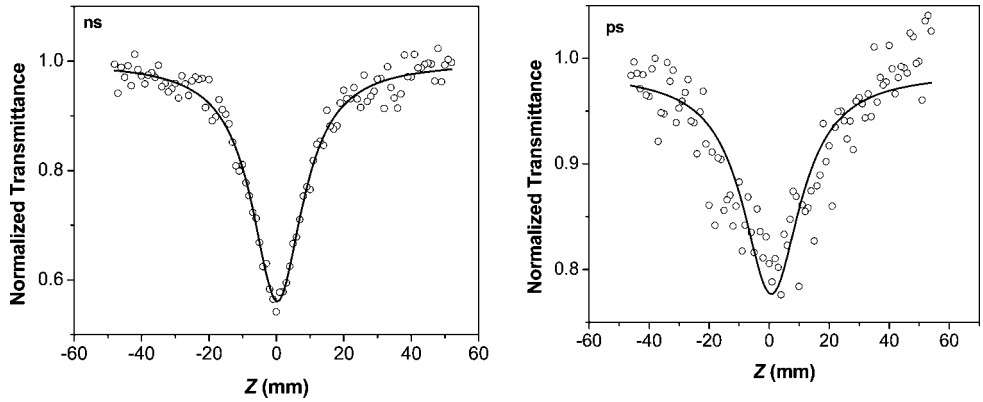

Figure 8. Normalized open-aperture data (open circles) and fitting curves (solid lines) for complex **2** at 532 nm. The energy used was 5.3 μJ for the nanosecond *Z*-scan and 3.9 μJ for the picosecond *Z*-scan, and the beam radius at the focal point was 32 μm for nanosecond *Z*-scan and 41 μm for the picosecond *Z*-scan.

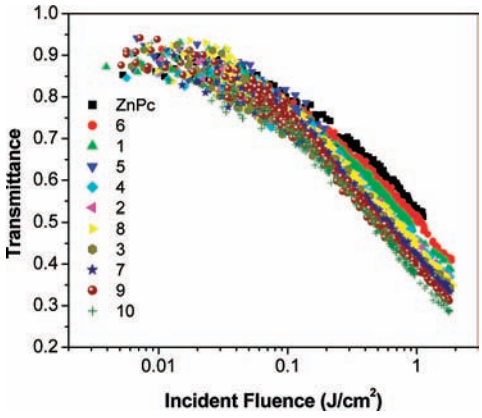

Figure 9. Nonlinear transmission curves for ZnPc derivatives and ZnPc at 532 nm for 4.1 ns (fwhm) laser pulses. The sequence of the legend labels goes from the worst nonlinear absorber (ZnPc) to the best one (complex **10**). The linear transmission for all samples was adjusted to 90% $\pm$ 0.2% in a 2 mm cuvette.

Figure 8 shows typical open-aperture curves for complex **2** using nanosecond and picosecond laser pulses at 532 nm, respectively. These curves clearly display a strong transmission decrease, indicating an RSA. In optically pumped chromophores in solution at room temperature, coherence effects are unimportant at time scales of a picosecond and longer; the population dynamics of such systems are well described by simple rate equation models described in the Experimental Section.[32] A single pair of excited-state absorption cross section values (σ_s, σ_T) that simultaneously fit both the nanosecond and picosecond *Z*-scans was obtained from the five-band model and the procedure described in the Experimental Section. The solid curves in Figure 8, which represent the best fit of the experimental data for complex **2**, were computed using the values 4.0×10^{-17} cm^2 for σ_s and 10.5×10^{-17} cm^2 for σ_T, corresponding to ratios of 16.7 for σ_s/σ_g and 43.8 for σ_T/σ_g at 532 nm. This confirms that the excited-state absorption cross section is much larger than that of the ground state. Therefore, the decrease of the transmission at the vicinity of the focal plane is indeed induced by RSA.

Table 2 lists the ground-state and excited-state absorption cross sections of the 10 ZnPc derivatives in DMSO measured by nanosecond and picosecond *Z*-scans at 532 nm. The magnitude of the ground-state absorption is of the order of 10^{-18} cm^2, whereas the excited-state absorption cross sections are of the order of 10^{-17} to 10^{-16} cm^2 at 532 nm. This gives a ratio of 8 to 19 for σ_s/σ_g and 11 to 308 for σ_T/σ_g at 532 nm. It is quite obvious that the α-tetrasubstituted complexes **7**−**10** possess much larger ratios of σ_T/σ_g than the monosubstituted ones (**1**−**5**) and the β-tetrasubstituted one (**6**) because of the larger excited-state absorption cross sections and the reduced ground-state absorption cross sections for **7**−**10** at 532 nm. In particular, the β-tetrasubstituted complex **6** has the smallest σ_T/σ_g ratio of 11 at 532 nm. In contrast, the σ_s/σ_g ratio at 532 nm does not vary significantly among these 10 complexes.

TABLE 3: Wavelength Dispersion of the Singlet Excited-State Absorption Cross Section for Complex 5 in DMSO Measured by Picosecond Open-Aperture *Z*-Scans

λ/nm	$\sigma_g/10^{-19}$ cm^2	$\sigma_s/10^{-17}$ cm^2	σ_s/σ_g
470	4.6	4.0 $\pm$ 0.8	87
500	5.5	3.2 $\pm$ 0.6	58
532	31.0	4.5 $\pm$ 0.5	15
550	76.0	4.0 $\pm$ 1.0	5

It is well-known that the nonlinear absorption is wavelength-dependent. To evaluate the wavelength dispersion of the nonlinear absorption, picosecond *Z*-scan experiments were conducted for two of these ZnPc derivatives in DMSO at multiple visible wavelengths. From 470 to 570 nm, both complexes exhibit an RSA. As exemplified in Table 3 for complex **5**, the excited-state absorption cross sections (σ_s) decrease at longer wavelengths. Meanwhile, the ground-state absorption cross sections increase at longer wavelengths. As a result, the ratio of σ_s/σ_g varies from 87 at 470 nm to 5 at 550 nm, corresponding to a factor of 17. A similar trend has been observed for complex **9**.

Nonlinear Transmission. As we discussed in the previous sections, these ZnPc derivatives show low ground-state absorption but strong triplet excited-state absorption from 400 to 580 nm. Especially, the open-aperture *Z*-scan experiments manifest the existence of RSA for both nanosecond and picosecond laser pulses at 532 nm. Therefore, it is expected that these complexes exhibit nonlinear transmission in this spectral region. To verify this, nonlinear transmission experiments were carried out at 532 nm using a Nd:YAG laser with a pulsewidth (fwhm) of 4.1 ns. As shown in Figure 9, all ZnPc derivatives exhibit a remarkable transmission decrease with increased incident fluence. The decrease in transmission of all 10 ZnPc derivatives with increasing fluence exceeds that of the unsubstituted ZnPc. The strength of the nonlinear transmission decreases in the following sequence: **10** > **9** > **7** > **3** > **8** > **2** > **4** > **5** > **1** > **6** > ZnPc. The α-tetrasubstituted complexes **7**−**10** generally exhibit stronger nonlinear transmission than do complexes **1**−**6**. In contrast, the β-tetrasubstituted complex **6** appears to be the weakest

nonlinear transmission suppressor among the 10 ZnPc derivatives, though its performance in this regard is still better than that of ZnPc. This trend is consistent with the prediction made on the basis of the nanosecond open-aperture *Z*-scan results. The incident fluence ("threshold") at which the transmittance falls to 50% of the linear transmittance is 1.34, 0.70, and 0.57 J/cm^2 for complexes **6**, **9**, and **10**, respectively. The enhanced degree of nonlinear transmission exhibited by these ZnPc derivatives should be attributed to their long triplet excited-state lifetimes and to their large values of the ratio of the excited-state absorption cross section to the ground-state absorption cross section.

Conclusion

The photophysical studies reveal that the peripheral-substituted ZnPc derivatives exhibit low ground-state absorption but strong triplet excited-state absorption from 400 to 580 nm with a longer triplet excited-state lifetime in comparison to the unsubstituted ZnPc. These complexes all exhibit RSA for nanosecond and picosecond laser pulses at 532 nm and show broad-band nonlinear absorption from 470 to 550 nm for picosecond laser pulses. Additionally, they all suppress the transmission of 532 nm nanosecond laser pulses better than ZnPc. Most importantly, our studies demonstrate that both the number and the position of the peripheral substituents dramatically affect the photophysics and nonlinear absorption of this type of materials. α-Tetrasubstitution causes bathochromic shifts in the ground-state absorption spectra, the fluorescence spectra, and the triplet transient difference absorption spectra, and it also enhances the triplet excited-state absorption coefficients and increases the ratios of the triplet excited-state absorption to the ground-state absorption cross sections. All these features suggest that the peripheral-substituted ZnPc derivatives are very promising nonlinear optical materials for applications that require strong and broad-band nonlinear absorption.

Acknowledgment. W. Sun acknowledges the financial support from the NSF NIRT program (DMI 0506531) and the Army Research Laboratory (W911NF-06-2-0032) and is grateful to Dr. Joy Rogers-Haley at UES Inc. and the Air Force Research Laboratory for her help in the singlet excited-state lifetime measurement. J. Huang acknowledges the financial support from the National Natural Science Foundation of China (Grant No. 20201005).

References and Notes

(1) Gregory, P. *J. Porphyrins Phthalocyanines* **2000**, *4* (4), 432.

(2) (a) Darwent, J. R.; Douglas, P.; Harriman, A.; Porter, G.; Richoux, M. C. *Photochem. Photobiol.* **1987**, *45*, 535. (b) Zuk, M. M.; Rihter, B. D.; Kenney, M. E.; Rodgers, M. A. J.; Kreimer-Birnbaum, M. *J. Chromatogr., B* **1991**, *568*, 437. (c) Jori, G. *J. Photochem. Photobiol., A* **1992**, *62*, 371. (d) Krasnovsky, A. A.; Rodgers, M. A.; Galpern, M. G.; Rihter, B.; Kenney, M. E.; Lukjanetz, E. A. *Photochem. Photobiol.* **1992**, *55*, 691. (e) Zuk, M. M.; Rihter, B. D.; Kenney, M. E.; Rodgers, M. A.; Kreimer-Birnbaum, M. *Photochem. Photobiol.* **1994**, *59*, 66. (f) Brasseur, N.; Nguyen, T. L.; Langlois, R.; Ouellet, R.; Marengo, S.; Houde, D.; Van Lier, J. E. *J. Med. Chem.* **1994**, *37*, 415. (g) Ford, W. E.; Rihter, B. D.; Kenney, M. E.; Rodgers, M. A. J. *J. Am. Chem. Soc.* **1989**, *111*, 2362. (h) Firey, P. A.; Ford, W. E.; Sounik, J. R.; Kenney, M. E.; Rodgers, M. A. J. *J. Am. Chem. Soc.* **1988**, *110*, 7626. (i) Marengo, S.; Houde, D.; Brasseur, N.; Nguyen, T. L.; Ouellet, R.; Van Lier, J. E. *J. Chim. Phys. Phys.−Chim. Biol.* **1994**, *91*, 1211.

(3) (a) Li, L.; Tang, Q.; Li, H.; Yang, X.; Hu, W.; Song, Y.; Shuai, Z.; Xu, W.; Liu, Y.; Zhu, D. *Adv. Mater.* **2007**, *19* (18), 2613. (b) Akazawa, T.; Takatsuka, Y.; Ohdaira, Y.; Shinbo, K.; Kato, K.; Kaneko, F. *Mol. Cryst. Liq. Cryst.* **2007**, *471*, 213. (c) Kelting, C.; Michaelis, W.; Hirth, A.; Woehrle, D.; Schlettwein, D. *J. Porphyrins Phthalocyanines* **2006**, *10*, 1179. (d) Liu, S.; Wang, W. M.; Mannsfeld, S. C. B.; Locklin, J.; Erk, P.; Gomez, M.; Richter, F.; Bao, Z. *Langmuir* **2007**, *23*, 7428. (e) Locklin, J.; Shinbo, K.; Onishi, K.; Kaneko, F.; Bao, Z.; Advincula, R. *Chem. Mater.* **2003**, *15*, 1404. (f) Bao, Z.; Lovinger, A. J.; Dodabalapur, A. *Appl. Phys. Lett.* **1996**, *69*, 3066.

(4) (a) Kluson, P.; Drobek, M.; Strasak, T.; Krysa, J.; Karaskova, M.; Rakusan, J. *J. Mol. Catal. A: Chem.* **2007**, *272* (1−2), 213. (b) Woehrle, D.; Suvorova, O.; Gerdes, R.; Bartels, O.; Lapok, L.; Baziakina, N.; Makarov, S.; Slodek, A. *J. Porphyrins Phthalocyanines* **2004**, *8* (8), 1020. (c) Iliev, V.; Tomova, D.; Bilyarska, L.; Prahov, L.; Petrov, L. *J. Photochem. Photobiol., A* **2003**, *159*, 281.

(5) (a) Makarov, N. S.; Rebane, A.; Drobizhev, M.; Wolleb, H.; Spahni, H. *J. Opt. Soc. Am. B* **2007**, *24* (8), 1874. (b) Seto, J.; Tamura, S.; Asai, N.; Kishii, N.; Kijima, Y.; Magsuzawa, N. *Pure Appl. Chem.* **1996**, *68* (7), 1429. (c) Makarov, N.; Drobizhev, M.; Rebane, A.; Peone, D.; Wolleb, H.; Spahni, H. *Proc. SPIE−Int. Opt. Soc. Eng.* **2006**, *6330*, 63300K/1.

(6) Nalwa, H. S.; Shirk, J. S. In *Phthalocyanines: Properties and Applications*; Leznoff, C. C., Lever, A. B. P., Eds.; VCH Publishers, Inc.: New York, 1996; Vol. 4, p 83.

(7) Micó, X. A.; Vagin, S. I.; Subramnian, L. R.; Ziegler, T.; Hanack, M. *Eur. J. Org. Chem.* **2005**, 4328.

(8) Chen, Y.; Hanack, M.; Araki, Y.; Ito, O. *Chem. Soc. Rev.* **2005**, *34*, 517.

(9) Torre, G. D. L.; Vazquez, P.; Agullo-Lopez, F.; Torres, T. *Chem. Rev.* **2004**, *104*, 3723.

(10) Gan, Q.; Li, S.; Morlet-Savary, F.; Wang, S.; Shen, S.; Xu, H.; Yang, G. *Opt. Express* **2005**, *13* (14), 5424.

(11) Nikolaitchik, A. V.; Korth, O.; Rodgers, M. A. J. *J. Phys. Chem. A* **1999**, *103*, 7587.

(12) Foley, S.; Jones, G.; Liuzzi, R.; McGarvey, D. J.; Perry, M. H.; Truscott, T. G. *J. Chem. Soc., Perkin Trans. 2* **1997**, 1725.

(13) Sastre, A.; Diaz-Garcia, M. A.; Rey, B. d.; Dhenaut, C.; Zyss, J.; Lendoux, I.; Agullo-Lopez, F.; Torres, T. *J. Phys. Chem. A* **1997**, *101*, 9773.

(14) Hanack, M.; Schneider, T.; Barthel, M.; Shirk, J. S.; Flom, S. R.; Pong, R. G. S. *Coord. Chem. Rev.* **2001**, *219*, 235.

(15) Kumar, G. A. *J. Nonlinear Opt. Phys. Mater.* **2003**, *12* (3), 367.

(16) Shirk, J. S.; Pong, R. G. S.; Flom, S. R.; Heckmann, H.; Hanack, M. *J. Phys. Chem. A* **2000**, *104*, 1438.

(17) Perry, J. W.; Mansour, K.; Lee, I. Y. S.; Wu, X. L.; Bedworth, P. V.; Chen, C. T.; Ng, D.; Marder, S. R.; Miles, P.; Wada, T.; Tian, M.; Sasabe, H. *Science* **1996**, *273*, 1533.

(18) Perry, J. W.; Mansour, K.; Marder, S. R.; Perry, K. J.; Alvarez, D., Jr.; Choong, I. *Opt. Lett.* **1994**, *19*, 625.

(19) Ho, Z. Z.; Ju, C. Y.; Hetherington, W. M., III *J. Appl. Phys.* **1987**, *62*, 716.

(20) Huang, J.; Ke, M. Synthesis of peripheral and nonperipheral substituted metallophthalocyanines. Chinese Patent Application No. 200710200223, Feb 16, 2007.

(21) Demas, J. N.; Crosby, G. A. *J. Phys. Chem.* **1971**, *75*, 991.

(22) Tran-Thi, T. H.; Desforge, C.; Thiec, C.; Gaspard, S. *J. Phys. Chem.* **1989**, *93*, 1226.

(23) Carmichael, I.; Gordon, L. H. *J. Phys. Chem. Ref. Data* **1986**, *15*, 1.

(24) Kumar, C. V.; Qin, L.; Das, P. K. *J. Chem. Soc., Faraday Trans.* **1984**, *280*, 783.

(25) Spiller, W.; Kliesch, H.; Wöhrle, D.; Hackbarth, S.; Röder, B.; Schnurpfeil, G. *J. Porphyrins Phthalocyanines* **1998**, *2*, 145.

(26) Oliveros, E.; Suardi-Murasecco, P.; Amian-Saghafi, T.; Braun, A. M.; Hansen, H.-J. *Helv. Chim. Acta* **1991**, *74*, 79.

(27) Wang, G.; Sun, W. *J. Phys. Chem. B* **2006**, *110* (42), 20901.

(28) Ogunsipe, A.; Chen, J.; Nyokong, T. *New J. Chem.* **2004**, *28*, 822.

(29) Stillman, M. J.; Nyokong, T. In *Phthalocyanines: Properties and Applications*; Leznoff, C. C., Lever, A. B. P., Eds.; VCH: New York, 1989; Vol. 1, pp 139−247.

(30) Bishop, S. M.; Beeby, A.; Meunier, H.; Parker, A. W.; Foley, M. S. C.; Phillips, D. *J. Chem. Soc., Faraday Trans.* **1996**, *92*, 2689.

(31) Kuznetsova, N.; Gretsova, N.; Kalmykova, E.; Makarova, E.; Dashkevich, S.; Negrimovskii, V.; Kaliya, O.; Luk'yanets, E. *Russ. J. Gen. Chem.* **2000**, *70*, 133.

(32) Hercher, M. *Appl. Opt.* **1967**, *6*, 947.

JP7108835